BEHAVIOR OF CIRCULAR CONCRETE COLUMNS REINFORCED WITH HOLLOW COMPOSITE SECTIONS AND GFRP BARS

Omar Alajarmeh[1*], Allan Manalo[1], Brahim Benmokrane[2], Wahid Ferdous[1], Ali Mohammad[1], Rajab Abousnina[1], Mohamed Elchalakani[3], Azam Edoo[4]

[1] University of Southern Queensland, Centre for Future Materials (CFM), School of Civil Engineering and Surveying, Toowoomba 4350, Australia

[2] University of Sherbrooke, Department of Civil Engineering, Sherbrooke 2500, Quebec, Canada

[3] The University of Western Australia, Faculty of Engineering and Mathematical Sciences, Perth 6009, Australia

[4] Composite Reinforcement Solutions Company, Perth 6162, Australia

Emails: Omar.Alajarmeh@usq.edu.au (corresponding author), Allan.Manalo@usq.edu.au, Brahim.Benmokrane@Usherbrooke.ca, Wahid.Ferdous@usq.edu.au, Ali.Mohammed@usq.edu.au, Rajab.Abousnina@gmail.com, mohamed.elchalakani@uwa.edu.au, azam@crsperth.com

ABSTRACT

Hollow concrete columns (HCCs) constitute a structurally efficient construction system for marine and offshore structures, including bridge piers and piles. Conventionally, HCCs reinforced with steel bars are vulnerable to corrosion and can lose functionality as a result, especially in harsh environments. Moreover, HCCs are subjected to brittle failure behavior by concrete crushing due to the absence of the concrete core. Therefore, this study investigated the use of glass fiber-reinforced polymer (GFRP) bars as a solution for corrosion and the use of hollow composite-reinforced sections (HCRSs) to confine the inner concrete wall in HCCs. Furthermore, this study conducted an in-depth assessment of the effect of the reinforcement configuration and reinforcement ratio on the axial performance of HCCs. Eight HCCs with the same lateral-reinforcement configuration were prepared and tested under monotonic loading until failure. The column design included a column without any longitudinal reinforcement, one reinforced longitudinally with an HCRS, one reinforced longitudinally with GFRP bars, three reinforced with HCRSs and different amounts of GFRP bars (4, 6, and 8 bars), and three reinforced with HCRSs and different diameters of GFRP bars (13, 16, 19 mm). The test results show that longitudinal reinforcement—whether GFRP bars or HCRSs—significantly enhanced the strength and displacement capacities of the HCCs. Increasing the amount of GFRP bars was more effective than increasing the bar diameter in increasing the confined strength and the displacement capacity. The axial-load capacity of the GFRP/HCRS-reinforced HCCs could be accurately estimated by calculating the load contribution of the longitudinal reinforcement, considering the axial strain at the concrete peak strength. A new confinement model considering the combined effect of the longitudinal and transverse reinforcement in the lateral confinement process was also developed.

Keywords: Hollow concrete column; GFRP bar; spiral; compressive load; lateral confinement; composite tube; design codes.

INTRODUCTION

Reinforced hollow concrete columns (HCCs) constitute a structurally efficient construction system for offshore and marine structures, including piles and bridge piers due to their high strength-to-mass ratio compared to solid columns with the same concrete area [1,2]. HCC structural behavior is controlled by a number of critical design parameters, including inner-to-outer diameter ratio, reinforcement ratio, volumetric ratio, and concrete compressive strength [3-7]. The reinforcement ratio (ρ) is the main parameter for increasing the strength capacity and axial stiffness of steel-reinforced HCCs [7]. Increasing the ρ has led to brittle failure due to the crushing of the unconfined inner concrete core. For instance, Hoshikuma and Priestley [7] increased the ρ from 1.45% to 3.18% by increasing the diameter of the longitudinal steel bars from 13 mm to 19 mm. While this increased the cyclic strength capacity by 58%, the ductility decreased by 52%. Likewise, Lee et al. [4] increased the ρ from 1.17% to 2.00% by increasing the amount of steel bars 24 mm diameter from 14 to 24 pieces, resulting in a 41% increase in the lateral flexural-strength capacity, but a 20% reduction in the displacement capacity. This was mainly due to the steel reinforcement, which stops contributing to the axial capacity after yielding, leading to crushing failure of the inner concrete core. A number of studies have also used concrete-filled steel tubes (CFSTs) [8,9,10] to improve HCC confinement strength and ductility. Steel corrosion, however, remains a main issue, rendering this technique unsuitable in marine and saline environments [11]. The corrosion issue leads to huge expenditures worldwide to retrofit and rehabilitate deteriorated members [12].

Currently, glass fiber-reinforced polymer (GFRP) reinforcement is considered a suitable alternative to steel reinforcement due to its superior environmental and mechanical properties. Recent in-field durability tests indicated no strength degradation nor chemical deficiency in the GFRP reinforcement in concrete structures [13, 14], even when the structures were exposed to harsh environmental conditions [15,16]. On the other hand, HCC behavior

was recently investigated by replacing the steel reinforcement with GFRP bars, which resulted in an overall enhancement in terms of overcoming the brittle behavior and maintaining strength in the post-peak stage [1, 17]. For example, Alajarmeh et al. [17] reinforced HCCs with 8 longitudinal GFRP bars instead of 4 to increase the ρ from 1.84% to 3.84%, resulting in 43% and 4% increases in the confined strength and displacement capacity. In the same study, the ρ was also increased from 1.79% to 4.00% by increasing the bar diameter from 13 to 19 mm, which led to 27% and 28% higher strength and ductility, respectively. This can be attributed to the linear elastic behavior of the GFRP bars with 4 to 5 times the strain capacity, and 2 to 3 times the ultimate strength of the steel bars. Consequently, the GFRP reinforcements were more effective in resisting the axial load than the steel ones in the post-peak stage until failure. The maximum reinforcement ratio that can be applied, however, is 4% [18] to avoid concrete segregation. For the same reason, the spacing between the lateral GFRP reinforcement, which is used to enhance strength through lateral confinement, is limited. Moreover, the cross section of HCCs is affected by the biaxial stress confinement, which evidences lower strength confinement than triaxial stress confinement [19]. Therefore, providing the inner hollow composite-reinforced section (HCRS) can significantly increase strength by providing a higher reinforcement ratio without causing concrete segregation and confining the inner concrete core triaxially.

This study aimed at investigating the performance of HCCs reinforced with various reinforcement ratios of longitudinal GFRP bars and reinforced internally with HCRSs (GFRP/HCRS-reinforced HCCs) under concentric axial compression. To achieve this, large-scale HCCs with different longitudinal reinforcement configurations and different amounts and diameters of GFRP bars were prepared and tested to determine the failure mechanisms and assess the load-displacement behavior, confined strength, and ductility of the test specimens. Empirical formulas were developed to estimate the design load capacity and predict the

confined strength of the new HCC design. This study is expected to provide a better understanding of the new reinforced HCC design as a structural system and yield test results that can be used in developing design standards for FRP-reinforced concrete columns.

EXPERIMENTAL PROGRAM

Materials

Four different material components were used to prepare the column specimens (see **Figure 1**), as follows:

a) Concrete (**Figure 1.a**)

Ready-mix concrete with 10 mm diameter coarse aggregate was used to cast all the column specimens. Eight concrete cylinders were prepared and tested on the same day as testing of the large-scale column specimens to measure the compressive strength in accordance with AS 1012.9 [20]. The average concrete compressive strength at 28 days was 30.2 MPa with a standard deviation of 2.7 MPa.

b) HCRS (**Figure 1.b**)

The hollow composite-reinforced sections (HCRSs) were manufactured by the pultrusion process, in which unidirectional glass fibers are impregnated with vinyl-ester resin. The fiber content was 73.2% by weight. **Figure 2.a** shows the cross section of the HCRSs, with a total area (A_R) of 1721 mm^2, including the flanges, which were designed to increase the contact with concrete. The axial compressive strength of the HCRSs was 120.4 MPa with a standard deviation of 5.8 MPa. Moreover, the modulus of elasticity (E_R) of the HCRSs was 32.2 GPa with a Poisson's ratio of 0.29, as obtained from **Figure 2.b**. These properties resulted from testing five HCRS tubes, in accordance to ASTM D695 [21]. Before testing, two strain gauges (3 mm in length) were mounted at the mid-height of the HSRC specimens to evaluate the stress–strain behavior of the HCRS (one gauge along the axis

and the other perpendicular to the axis). **Figure 2.b** shows the stress–strain diagram, in which the observed final mode of failure occurred as crushing at either the top or bottom side of the HCRS. This composite section was supplied by Composite Reinforcement Solutions in Perth, Australia.

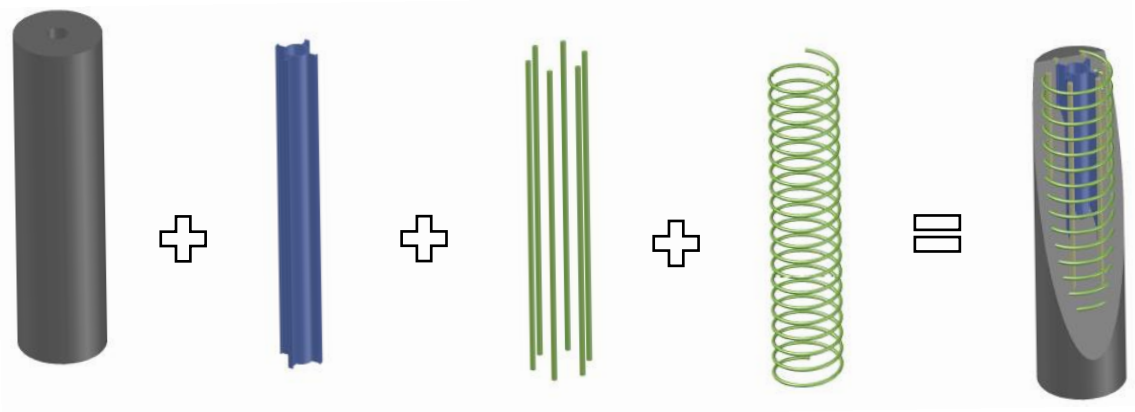

a) Hollow plain concrete | b) HCRS | c) GFRP bars | d) GFRP spirals | GFRP/HCRS-reinforced HCC

Figure 1. Materials used in fabricating the column specimens

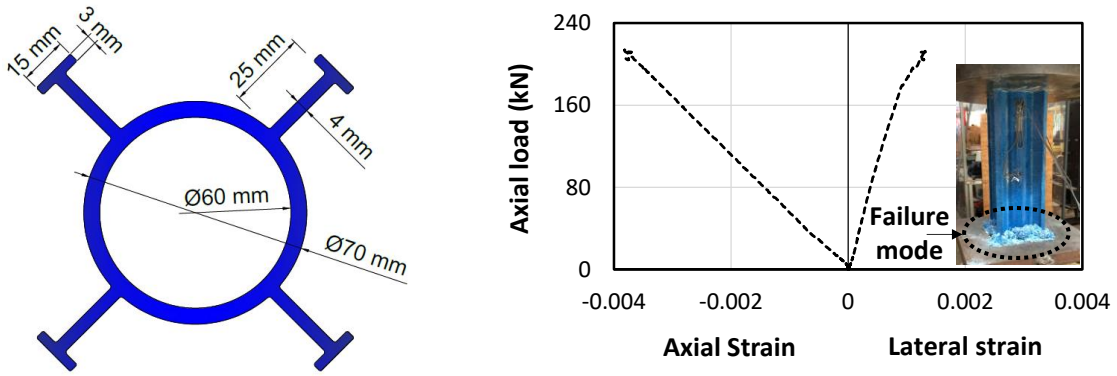

a. HCRS cross section **b.** HCRS stress–strain behavior

Figure 2. HCR S cross-section and stress-strain behavior

c) Longitudinal GFRP bars (**Figure 1.c**)

Sand-coated High Modulus GFRP bars made with E-glass fibers and modified vinyl-ester resin. Bars with three nominal diameters (13, 16, and 19 mm) were used as longitudinal reinforcement. **Table 1** provides the mechanical and physical properties of the longitudinal

bars. Their properties were tested in accordance with CSA S806 [22] and ASTM D7205 [23].

Table 1. Mechanical and physical properties of the GFRP reinforcement

	Property	Test Method	Number of Specimens	Longitudinal Bars			Spirals
				No. 19	No. 16	No. 13	No. 10
Physical	Nominal bar diameter, d_b (mm)	CSA-S806 Annex A [22]	9	19.1	15.9	12.7	9.5
	Nominal bar area†, A_b (mm^2)		9	286.5	198.5	126.6	70.8
	Bar cross-sectional area by immersion test (mm^2)			317.3 (1.9)*	224.4 (1.2)*	145.0 (1.7)*	83.8 (1.9)*
Mechanical	Ultimate tensile strength, f_u (MPa)	ASTM D7205/D7205M-06 [23]	6	1270.0 (31.4)*	1237 (33.3)*	1281.5 (35.3)*	1315 (31.1)*
	Modulus of elasticity, E_b (GPa)		6	60.5 (0.5)*	60.0 (1.3)*	61.3 (0.4)*	62.5 (0.4)*
	Ultimate strain, ε_u(%)		6	2.1 (0.1)*	2.1 (0.1)*	2.1 (0.1)*	2.3 (0.1)*

† The adopted area for calculating mechanical properties
* Standard deviation

d) Lateral GFRP spirals (**Figure 1.d**)

The lateral GFRP spirals had the same properties and manufacturing process as the longitudinal GFRP bars, but a smaller bar diameter (9.5 mm or #3) (see **Table 1**). Due to the curvature of the GFRP spirals, the ultimate tensile strength ($f_u = 1315MPa$) was reduced to the effective tensile strength ($f_{bent} = 1052MPa$), which was calculated with Eq. (1) as recommended in ACI 440.1R [24].

$$f_{bent} = \left(0.05\frac{r}{d_b} + 0.3\right) f_u \leq f_u \qquad \text{Eq. (1)}$$

where r is the radius of curvature (95 mm) and d_b is the spiral nominal diameter (9.5 mm).

Specimen Design

Eight columns 1 m in height with an outer diameter of 250 mm were prepared and tested. The size of the specimens was based on the equipment's loading capacity of 2500 kN. The diameter of the inner void in all column specimens was 65 mm, which is comparable to the specimens reinforced with HCRSs (**Figure 2.a**). All column specimens were laterally reinforced with GFRP spirals spaced on 50 mm centers to ensure sufficient lateral confinement for the concrete core after crushing of the concrete cover [25-27]. The tested column specimens were divided into three groups (**Figure 3**). Group 1 (**Figure 3.a**) was to determine the effect of using different reinforcement materials and configurations on the HCCs and to investigate the effect of confining the inner void with HCRSs under the axial compression. Group 2 (**Figure 3.b**) was to determine the effect of the reinforcement ratio with different amounts of longitudinal GFRP bars (4, 6, 8, and 16 mm in diameter). Group 3 (**Figure 3.c**) aimed at showing the effect of the reinforcement ratio with different bar diameters (13 mm, 16 mm, and 19 mm). The amounts and diameters of the longitudinal bars were selected to limit the reinforcement ratio to between 1% and 4%, in accordance with AS 3600 [18]. **Table 2** shows the design matrix of the column specimens and the reinforcement details. The column specimen labels consist of three letters: H for hollow column; G or N for with or without longitudinal GFRP bars; and C or N for with or without HCRS. The letters are followed by numbers representing the amount and diameter of the longitudinal GFRP bars. For example, HGC-8-16 is a GFRP/HCRS-reinforced hollow column with 8 GFRP bars 16 mm in diameter. Similarly, HNN-0-00 is a hollow column without any longitudinal reinforcement.

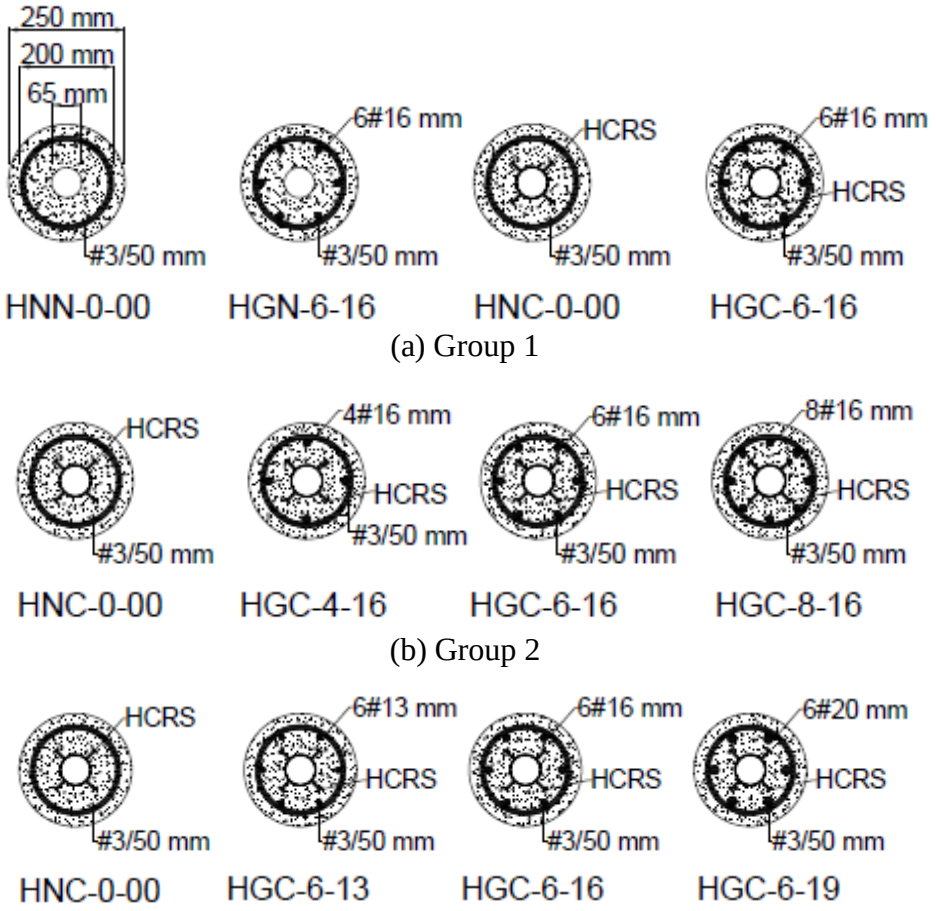

Figure 3. Specimen cross section

Table 2. Design matrix of the column specimens

Specimen Label	GFRP Bars	HCRS	Number of Longitudinal Bars	Bar diameter (mm)	Reinforcement Ratio*, ρ (%)
HGC-6-13	Yes	Yes	6	13	1.66
HGC-6-16 †	Yes	Yes	6	16	2.60
HGC-6-19	Yes	Yes	6	20	3.76
HGC-4-16	Yes	Yes	4	16	1.73
HGC-8-16	Yes	Yes	8	16	3.47
HGN-6-16	Yes	No	6	16	2.60
HNC-0-00 †	No	Yes	0	-	0.00
HNN-0-00	No	No	0	-	0.00

* Excluding the HCRS. † Common specimens in each group (**Figure 3**).

Test Setup and Instrumentation

The columns were tested under monotonic axial loading with a 2500 kN hydraulic jack. Prior to casting the concrete, two uniaxial strain gauges (3 mm in length) were mounted each on the longitudinal bars (along the longitudinal axis), spirals (along the lateral axis), and HCRS (in the hoop direction). Two strain gauges (20 mm in length) were also glued vertically on the outer surface of the concrete at column mid-height. **Figure 4.a** shows the instrumentation at the mid-height cross-section of the columns. The top and bottom 100 mm of the columns were wrapped in double layers of GFRP sheets along the direction of the longitudinal fibers to prevent the premature failure caused by stress concentration during the axial compression loading. For the same reason, steel clamps 50 mm in width and 10 mm in thickness were also attached at the top and bottom of the column specimens. Moreover, neoprene rubber pads 3 mm in thickness were placed between the steel plates and the top and bottom surfaces of the column specimens for uniform load distribution (see **Figure 4.b**). During the test, the applied load was measured with a load cell with a 2500 kN capacity, while the axial displacement was recorded with a string pot. All column specimens were tested under a constant loading rate of 2 mm/min until failure. Moreover, a System 5000 data logger was used to record load, strain, and axial displacement. In addition, crack propagation and failure were video-recorded throughout testing.

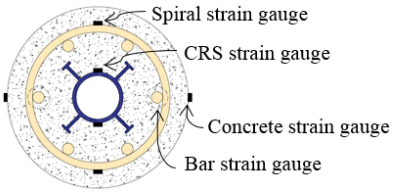

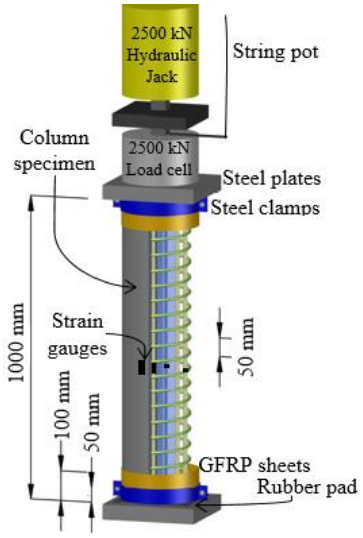

(a) Mid-height cross section (b) Test setup

Figure 4. Instrumentation and test setup

TEST RESULTS AND DISCUSSION

Group 1

Failure mode

Generally, the progression of failure in Group 1 columns started with hairline cracks initiating at the mid-height of the outer surface of the concrete, which propagated along the entire column height at advanced loading levels. Afterwards, the concrete cover started to spall off as the result of an intact concrete core confined by the discrete GFRP spirals. The final failure mode for this group varied, however, based on the presence and type of longitudinal reinforcement. For example, column HNN-0-00 experienced only failure of the concrete core, where concrete crushing was observed between the discrete GFRP spirals with no failure at the spirals (**Figure 5.a**). This mode of failure was controlled by the partial lateral confinement of the concrete core ceased between the lateral GFRP spirals. Sankholkar [28] made similar observations for solid GFRP-reinforced columns reinforced with only GFRP spirals. Providing the HCRS in column HNC-0-00 yielded concrete core degradation similar to that of column HNN-0-00 with, however, fracture of the lateral spiral (**Figure 5.b**). This behavior is due to the increase in column axial stiffness provided by the HCRS. This produced increased stored energy, which led to a more aggressive failure at a higher level of confined strength and ended with a fracture in the lateral spiral. On the other hand, using only the GFRP bars as longitudinal reinforcement in column HGN-6-16 exhibited crushing failure of these bars and fracturing of the lateral GFRP spirals (see **Figure 5.c**). The longitudinal GFRP bars were able to produce an additional lateral confinement with the GFRP spirals by covering more unconfined concrete core, limiting the failure to the GFRP reinforcement. Alajarmeh et al. [1] had observed the same mode of failure for GFRP-reinforced HCCs. Lastly, providing a combination of longitudinal GFRP bars and

HCRS in column HGC-6-16 limited the final failure to the top portion of the column (**Figure 5.d**). This failure can be described as the crushing of the longitudinal GFRP bars and the HCRS at the top face of the column only and the smashing of the surrounding concrete. Afterwards, this mode ended either with fracturing in the lateral spirals or losing the surrounding concrete. This mode occurred even with the high amount of the lateral confinement provided by the GFRP sheets and steel caps. The HCRS was primarily responsible for initiation of this failure, with localized failure occurring at the ends at high load levels (**Figure 2.b**). This localized failure concentrated the stresses around the top portion of the column. When longitudinal GFRP bars were used, the HCRS flanges contributed significantly to this mode of failure, providing good contact with the surrounding concrete, and the HCRS's high sectional geometry preventing failure anywhere else. A similar mode of failure was observed for the pultruded sections under compression [29]. Moreover, Fam and Rizkallah observed the same mode of failure for concrete-filled circular FRP tubes [30].

a. HNN-0-00 b. HNC-0-00 c. HGN-6-16 d. HGC-6-16

Figure 5. Final modes of failure for the columns in Group 1

Axial load–axial displacement behavior

Figure 6 shows the axial load–displacement behavior of the Group 1 columns. All of the column specimens generally displayed a linear ascending load–displacement behavior up until the first axial peak load (P_1) (denoted by the ◊ in **Figure 6**). **Figure 6** clearly shows that the linear ascending behavior of the slope (axial stiffness) of the columns in Group 1 differed slightly based on the presence and type of longitudinal reinforcement. For example, providing the HCRS slightly increased the axial stiffness of the linear ascending part of the load–displacement line by 4.7% compared to column HNN-0-00. This increase is very close to the axial stiffness of the HCRS ($E_R \times A_R = 55416kN$) proportioned to the total stiffness of the hollow column ($E_b \times A_b = 1337632kN$) by 4.2%. Providing longitudinal GFRP bars at a reinforcement ratio (ρ) of 2.6% increased the axial stiffness by 6.9% compared to column HNN-0-00. The difference in the axial stiffness between columns HGN-6-16 and HNN-0-00 is also close to the proportioned stiffness between the longitudinal GFRP bars ($71640\ \mathrm{kN/mm^2}$) and the concrete column ($1337632\ \mathrm{kN/mm^2}$) For column HGC-6-16, providing longitudinal GFRP bars and HCRS increased the axial stiffness by 10.0% compared to column HNN-0-00. The increase is predictable given the additional reinforcement ($(55416 + 71640)/1337632 = 9.5\%$).

Just before P_1, short nonlinear ascending behavior was observed in all Group 1 columns, caused by the propagation of the hairline cracks up until P_1. P_1 is the load-carrying contribution of the concrete (mostly) and the longitudinal reinforcement. Considerable enhancement on the P_1 can be found for the GFRP and/or HCRS-reinforced HCCs compared to column HNN-0-00. Columns HNC-0-00, HGN-6-16, and HGC-6-16 showed 22.7%, 23.1%, and 31.4% higher P_1, respectively, than column HNN-0-00. This increase resulted from providing longitudinal reinforcement (GFRP bars and HCRS). This increase was greater than that predicted (15.4%, 13.5%, and 28.9%, respectively). The predicted values considered the individual contributions

of the longitudinal reinforcement by multiplying its area and modulus of elasticity with the axial strain at P_1 (ε_{b,P_1}, **Table 3**). This behavior shows that the longitudinal reinforcement added to the section's axial stability, evidenced by the reduction in the lateral expansion of the section (see ε_{s,P_1} values in **Table 3**). This delayed the crack propagation in the concrete, as indicated by the higher concrete strain at P_1 with the increase in longitudinal reinforcement (see ε_{c,P_1} values in **Table 3**). As shown in the table, the GFRP bars as longitudinal reinforcement were more effective in increasing P_1 than the HCRS. This finding relates mainly to the location of the GFRP bars that contributed also in confinement of concrete, preventing the concrete from expanding laterally once the columns started to show the nonlinear behavior.

A 4% to 7% load drop in P_1 can be observed at the post-peak stage, due to the end of the concrete cover crushing. An ascending behavior was then observed due to the activation of the lateral confinement by the GFRP spirals: the higher the axial reinforcement stiffness, the lower the load drop. The axial stiffness of the post-peak behavior was less than in the elastic stage due to the significant reduction of the concrete stiffness after it reached its peak strength. This stage, however, is mainly controlled by the type and configuration of longitudinal reinforcement. For example, column HNN-0-00 showed a nearly stable load resistance in the post-peak stage as the concrete had already reached its maximum axial resistance. The lateral confinement provided by the spirals delayed the final failure of the concrete-core crushing (**Figure 5.a**). Columns HNC-0-00 and HGN-6-16 showed higher post-peak behavior than HNN-0-00 due to the increase in the axial stiffness provided by the longitudinal reinforcement. Providing GFRP bars was, however, more effective than providing HCRS due to the GFRP bars having greater mechanical properties than the HCRS (see **Table 1** and **Figure 2**). Moreover, the location and arrangement of the GFRP bars increased the lateral confinement and prevented the concrete core from failing. The post-peak behavior ended with a second peak load (P_2) (denoted by the ○ in **Figure 6**), representing the column's maximum confined strength

(f'_{cc}). The f'_{cc} was calculated by dividing P_2 by A_e, where A_e is the area of the concrete core measured from the diameter of the spiral centers. Adding longitudinal reinforcement increased f'_{cc} due to higher axial stiffness. Therefore, column HGC-6-16 had a f'_{cc} 87.1%, 44.9%, and 44.5% higher than columns HNN-0-00, HNC-0-00, and HGN-6-16, respectively. On the other hand, column HNC-0-00 evidenced 12.4% higher displacement capacity or ductility (DF) than column HNN-0-00. This is due to column HNC-0-00 having higher the axial stiffness due to the HCRS, delaying failure and contributing to axial deformation. This behavior also emphasizes that the HCRS functioned as longitudinal reinforcement. DF was then calculated by dividing the axial displacement corresponding to the P_2 (Δ_u) by the axial displacement corresponding to the P_1 (Δ_y). This approach was also by Alajarmeh et al. [17] adopted for the GFRP-reinforced HCCs. Noticeably, column HGN-6-16 had significantly higher DF than column HNC-0-00 (101.3%). This emphasizes the crucial role of the location and arrangement of the longitudinal GFRP bars in increasing lateral confinement. In contrast, column HGC-6-16 had 47.6% lower DF than column HGN-6-16. This might be due to the almost double increase in reinforcement ratio, which increased column axial stiffness. This approach, however, also resulted in brittle failure behavior, indicating that the energy restoration capacity within the section should be high enough to reduce the lateral expansion of the concrete section. Further evidence for this finding is provided by the lower strain values in the lateral GFRP spirals at P_2 (see ε_{s,P_2} values in **Table 3**). After P_2, the columns showed a gradual loss in axial-load resistance, resulting in the failure load point (P_f), which produced the final failure mode, as previously described in **Figure 5**.

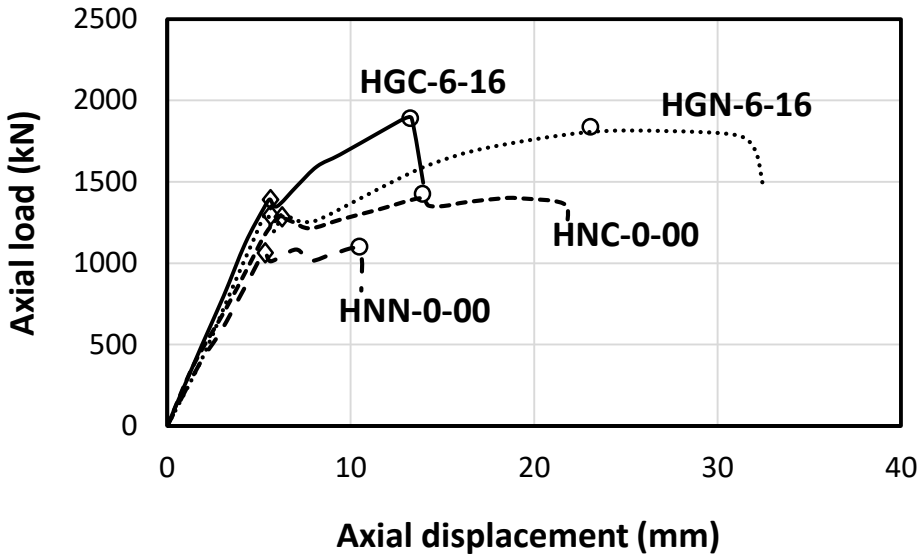

Figure 6. Load–displacement behavior of the columns in Group 1

Table 3. Test results of the column specimens

Specimen	Stiffness (kN/mm)	P_1 (kN)	Δ_y (mm)	P_2 (kN)	Δ_u (mm)	P_f (kN)	*DF*	f'_{cc} (MPa)	ε_{c,P_1} ($\mu\varepsilon$)	ε_{b,P_1} ($\mu\varepsilon$)	ε_{b,P_2} ($\mu\varepsilon$)	ε_{s,P_1} ($\mu\varepsilon$)	ε_{s,P_2} ($\mu\varepsilon$)
HNN-0-00	211	1060	5.6	1084	10.8	1062	1.93	43.3	1791	-	-	1133	9227
HNC-0-00	221	1301	6.5	1400	14.1	1369	2.17	55.9	2001	-	-	856	8726
HGN-6-16	226	1305	5.2	1804	22.7	1693	4.37	72.1	1999	2054	10172	670	7294
HGC-6-16	232	1393	5.9	1903	13.5	1891	2.29	76.0	1932	2039	8556	463	6082
HGC-4-16	227	1382	7.4	1597	17.1	1381	2.31	63.8	1808	1874	7413	752	3902
HGC-8-16	235	1321	5.7	2096	18.0	1923	3.16	83.7	1825	2175	9451	562	4086
HGC-6-13	229	1363	6.5	1900	15.5	1717	2.38	75.9	2224	2320	9930	617	6141
HGC-6-19	244	1549	7.6	2119	15.5	1935	2.04	84.6	1746	2264	7833	899	3901

Axial load–strain behavior

Figure 7 shows the axial load–strain behavior of the GFRP bars, spirals, and HCRS in Group 1 columns. **Table 3** reports the maximum strain of the concrete and the strain values of the GFRP bars and spirals at P_1 and P_2. In **Figure 7**, the plots for the GFRP bars show linear ascending behavior until P_1 was reached. The axial strain of the GFRP bars in Group 1 columns at P_1 (ε_{b,P_1}) was almost 0.002. This value is very close to the maximum recorded axial strain in the concrete (ε_{c,P_1}) (see **Table 3**), indicating that P_1 was primarily controlled by the concrete's peak strength. Similar to the longitudinal GFRP bars, the lateral GFRP spirals showed linear elastic behavior until P_1 but with lower strain values (ε_{s,P_1}) ranging from 0.0007 to 0.0011. Although the upper

bound of ε_{s,P_1} was less than 5% of the ultimate tensile strain, the lateral confinement by the spirals was still ineffective at P_1, and the value of ε_{s,P_1} was slightly affected by the amount of the longitudinal reinforcement. Therefore, lower ε_{s,P_1} values were observed for the columns with longitudinal reinforcement with higher axial stiffness, which reduced the lateral expansion of the concrete section. Alajarmeh et al. [17] made similar observations. It should be noted that the proportion of the lateral and axial strain readings at P_1 is around 0.45, which represents the Poisson's ratio of the concrete at its peak [31]. On the other hand, strain gauges mounted on the HCRS in HNC-0-00 and HGC-6-16 exhibited similar behavior to the GFRP spirals (see **Figure 7**). This finding reveals that the whole cross section was expanding towards the outside under the effect to the Poisson's ratio until P_1 was reached. This contradicts the assumption made by Cascardi et al. [32] that the outer face of hollow columns expanded outward, while the inner face always contracted inward at all loading levels.

A significant increase in the strain readings of the longitudinal bars coincided with the decrease in axial-load capacity caused by the concrete cover crushing. This sudden increase expresses the significant loss of the concrete axial stiffness and the load-resistance capacity of the outer concrete cover. The strain in the GFRP spirals also significantly increased, while the axial-load resistance decreased due to the excessive lateral expansion of the concrete after reaching P_1. This increase was due to the activation of the lateral confinement, which prevented or delayed the concrete core from failing. On the other hand, an inflection point in HCRS behavior occurred at P_1, where the stress in the HCRS changed from tension to compression. Fam and Rizkalla [29] noted this typical behavior in HCCs made with plain concrete and fully wrapped in CFRP sheets. It was due to the concrete starting to expand excessively in both directions after reaching peak strength (concrete plastic behavior), which caused compressive strain in the HCRS and tensile strain in the GFRP spirals.

According to **Figure 7**, the ultimate recorded compressive strain in the longitudinal GFRP bars (ε_{b,P_2}) was 0.011 for column HGN-6-16. This represents 52.3% of the ultimate tensile strain of the GFRP bars and is consistent with the value reported by Alajarmeh et al. [17] for GFRP bars in concrete columns under compression. Moreover, **Figure 7** shows the significant increase in axial strain in the GFRP spirals, which prevented failure of the concrete core and buckling of the longitudinal GFRP bars as well as resulting in P_2 being higher than P_1. The maximum axial strain in the GFRP spirals was 0.0092 (column HNN-0-00), representing 51.8% of the ultimate tensile strain of the bent GFRP bars. According to **Figure 7**, the ε_{s,P_2} values noticeably decreased as the longitudinal reinforcement increased by providing GFRP bars and/or HCRS. For example, the cross-sectional lateral expansion column HGC-6-16 was 34.1% less than in column HNN-0-00. As mentioned above, this was mainly due to increased column axial stiffness as the result of increasing the reinforcement ratio. Interestingly, none of the strain readings for the HCRS reached the ultimate concrete compressive strain (0.003 [33]), which indicates that no crushing occurred in the inner concrete wall. Moreover, the low strain values at the inner face of the hollow section in the hoop direction imply that the HCRS was acting primarily as longitudinal reinforcement rather than confining the HCC's inner face.

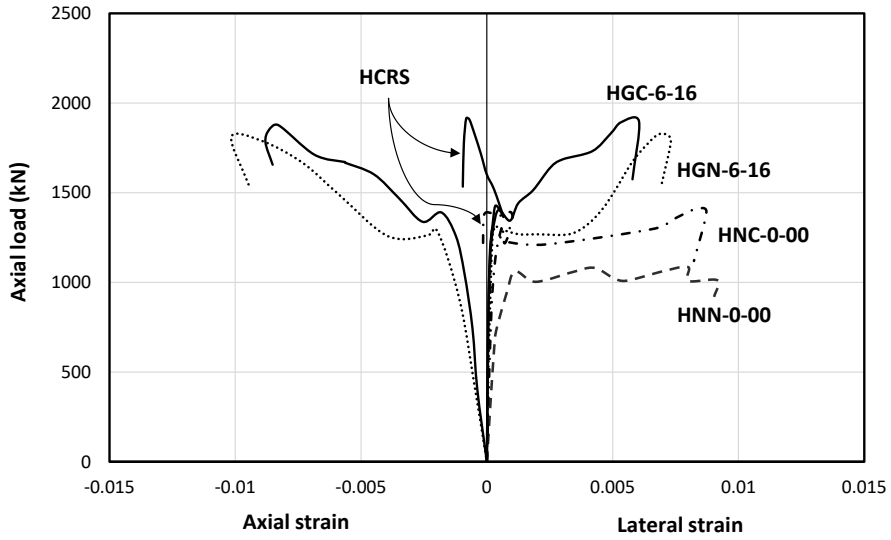

Figure 7. Axial load–strain behavior of the GFRP bars, spirals, and HCRS in Group 1

Group 2

Failure mode

The columns in Group 2 failed differently depending on the presence and number of longitudinal GFRP bars. As seen in **Figure 8.a**, column HNC-0-00 exhibited distributed cracks along the height and bulging in the cross-section close to column mid-height, indicating lateral expansion of the concrete core in the post-peak stage. This type of failure ended with a fracture in the lateral GFRP spirals (see **Figure 5.b**). On the other hand, providing GFRP bars and HCRS as longitudinal reinforcement in the HCC exhibited almost similar final mode of failure as that in **Figure 5.d** due to the high cross-sectional reinforcement ratio. This specimen failed due to localized failure of the HCRS, as shown in **Figure 2.b**. Increasing the amount of GFRP bars, however, had a clear effect on the failure progression. Column HGC-4-16 had a significantly wide, inclined longitudinal crack, followed by lateral cross-sectional expansion, which ended with crushing in the top portion of the column. The wide spacing between the longitudinal GFRP bars was the responsible for this cracking pattern in the outer concrete cover, where the inclined crack was limited to one-quarter of the column, as shown in **Figure 8.b**. Using 6 bars instead of 4 in column HGC-6-16 increased the number of cracks in different

directions, indicating that the cracks propagated in more progressively compared to column HGC-4-16, as evidenced by the thinner cracks (see **Figure 8.c**). Column HGC-8-16 exhibited many hairline cracks on the top portion of the column just beneath the GFRP sheets (see **Figure 8.d**), which developed and propagated downward and resulted in overall crushing of the concrete cover. This was due to the high amount of GFRP bars and spirals between the concrete core and the outer concrete cover.

a. HNC-0-00 b. HGC-4-16 c. HGC-6-16 d. HGC-8-16

Figure 8. Failure progression of the columns in Group 2

Axial load–axial displacement behavior

A short but expected increase in the axial stiffness values were observed in the linear elastic stage (see **Figure 9** and **Table 3**) due to the increase in the number of longitudinal GFRP bars (0, 4, 6, or 8). Providing 4 GFRP bars in column HGC-4-16 resulted in a 5.5% increase in P_1 compared to column HNC-0-00 due to the load-carrying contribution of the longitudinal GFRP bars. In contrast, column HGC-6-16 evidenced an insignificant increase in P_1 compared to column HGC-4-16. On the other hand, the P_1 of column HGC-8-16 4.4% was lower than that of column HGC-4-16. This unexpected finding might be related to the increase in the number of longitudinal GFRP bars, producing greater separation between the concrete core and cover. This behavior led to early cracking of the outer concrete cover, resulting in stability failure

instead of crushing failure in the concrete cover. Hadi et al. [34] reported similar observations with GFRP-reinforced solid concrete columns with reduced spacing between the lateral reinforcement. A drop in the axial-load resistance was observed due to concrete cover crushing (**Figure 9)**. Columns HNC-0-00, HGC-4-16, HGC-6-16, and HGC-8-16 showed 5.0%, 8.1%, 3.3%, and 2.5% drops in P_1, respectively. There is a positive correlation between the axial stiffness of the columns with longitudinal GFRP reinforcement and maintaining axial-load capacity. The role played by the GFRP bars in maintaining axial-load capacity is evidenced by the significant strain increase in the longitudinal GFRP bars just after P_1 (**Figure 10**). This finding also supports the wide separation between the concrete cover and core with greater amounts of GFRP bars. In contrast, using only 4 longitudinal GFRP bars yielded more contact area between the concrete cover and core. Therefore, more of the concrete core spalled off with the concrete cover after P_1, which led to higher axial-load decay, as shown in **Figure 9**. It should be mentioned that, even after the load drop, HGC-4-16 (4 longitudinal bars) had 3% more axial-load resistance than column HNC-0-00.

After the load drop, the confinement was activated, providing load resistance until failure, as shown in **Figure 9**. The presence of the GFRP bars and increased number of bars affected the stiffness of the ascending behavior in the post-peak stage: column HGC-8-16 had 3%, 5%, and 11% higher axial stiffness than columns HGC-6-16, HGC-4-16, and HNC-0-00, respectively. Moreover, the high axial stiffness of the longitudinal reinforcement in column HGC-8-16 yielded confined strength (f'_{cc}) 10.1%, 31.2%, and 49.7% higher than columns HGC-6-16, HGC-4-16, and HNC-0-00, respectively. This can be attributed to the longitudinal reinforcement having greater axial-load carrying capacity and higher lateral confinement as they covered more of the unconfined concrete core between the lateral spirals. For the same reason, column HGC-8-16 had 38.0%, 36.8%, and 45.6% higher displacement capacity (DF) than columns HGC-6-16, HGC-4-16, and HNC-0-00, respectively. Moreover, HGC-6-16 had

in 1% lower DF than its counterpart (column HGC-4-16), despite having more longitudinal GFRP bars. This finding might be due to the wide spacing between the longitudinal GFRP bars in the latter column, allowing for easier crushing and degradation of the concrete core, resulting in more axial displacement. In addition, this finding is supported by the lower effectiveness of the lateral confinement in column HGC-4-16, as evidenced by the lower strain values in the GFRP spirals at the maximum confined-strength point (ε_{s,P_2}) (**Table 3** and **Figure 6**). Increasing the amount of longitudinal GFRP bars enhanced the post-peak stage, including load decay, displacement capacity, and confined strength, all of which is consistent with what Alajarmeh et al. [17] found for GFRP-reinforced hollow concrete columns with different numbers of longitudinal GFRP bars, but no internal HCRS.

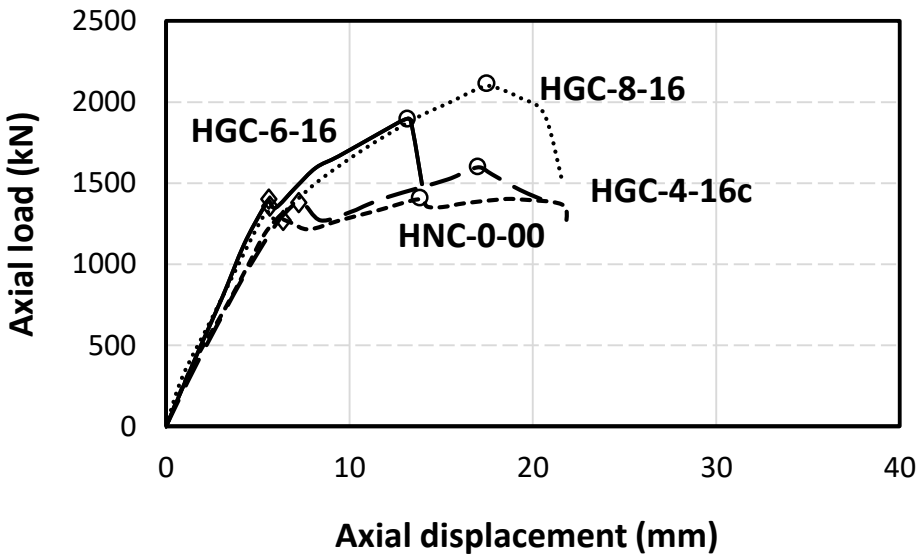

Figure 9. Load-displacement behavior of the column specimens in Group 2

Axial load–strain behavior

Figure 10 shows the axial load–strain behavior of the GFRP bars, spirals, and the HCRS in the Group 2 columns. **Table 3** gives the maximum strain values of the concrete and the strain values of the GFRP bars and spirals at P_1 and P_2. Similar to what it in **Figure 7**, the GFRP

longitudinal bars showed linear ascending behavior until reaching P_1 with an average strain between 0.0019 and 0.0022. In contrast, the axial concrete strain at P_1 (ε_{c,P_1}) ranged between 0.0018 and 0.0020. These strain values are slightly higher than those for Group 1. This finding relates to the higher axial stability of the concrete section caused by the greater number of longitudinal GFRP bars, which delayed expansion of the concrete. This observation is also supported by the strain reading in the lateral GFRP spirals (ε_{s,P_1}), which was less than 4% of the ultimate tensile strain. Moreover, the tensile-strain readings in the HCRS were almost equal to that of the GFRP spirals up until P_1, and were similar to that observed for Group 1. **Figure 10** reveals a significant increase in the strain readings for both the GFRP bars and spirals after P_1 (representing the post-peak stage). As mentioned above, this increase maintained the column's axial-load capacity after the concrete reached its peak strength, then tending to fail afterwards. After P_1, the HCRS in Group 2 showed an inflection towards the compression side, indicating contraction pressure of the concrete towards the center of the section. Nevertheless, the maximum compressive strain was barely 0.001, indicating a slight contraction response of the inner concrete wall. This behavior might be due to the arch effect, which converts the inward lateral in-plane contraction in the concrete wall into compression stresses in the circumferential direction. Consequently, the HCRS acted primarily as longitudinal reinforcement. As shown in **Figure 10**, increasing the number of longitudinal GFRP bars increased the section's axial stability, which increased the axial contribution, as evidenced by the higher axial strain readings (ε_{b,P_2}). On the other hand, increasing the section's axial stiffness decreased the section's lateral expansion, as indicated by the lower lateral strain readings in the GFRP spirals (ε_{s,P_2}) (see **Table 3** and **Figure 10**).

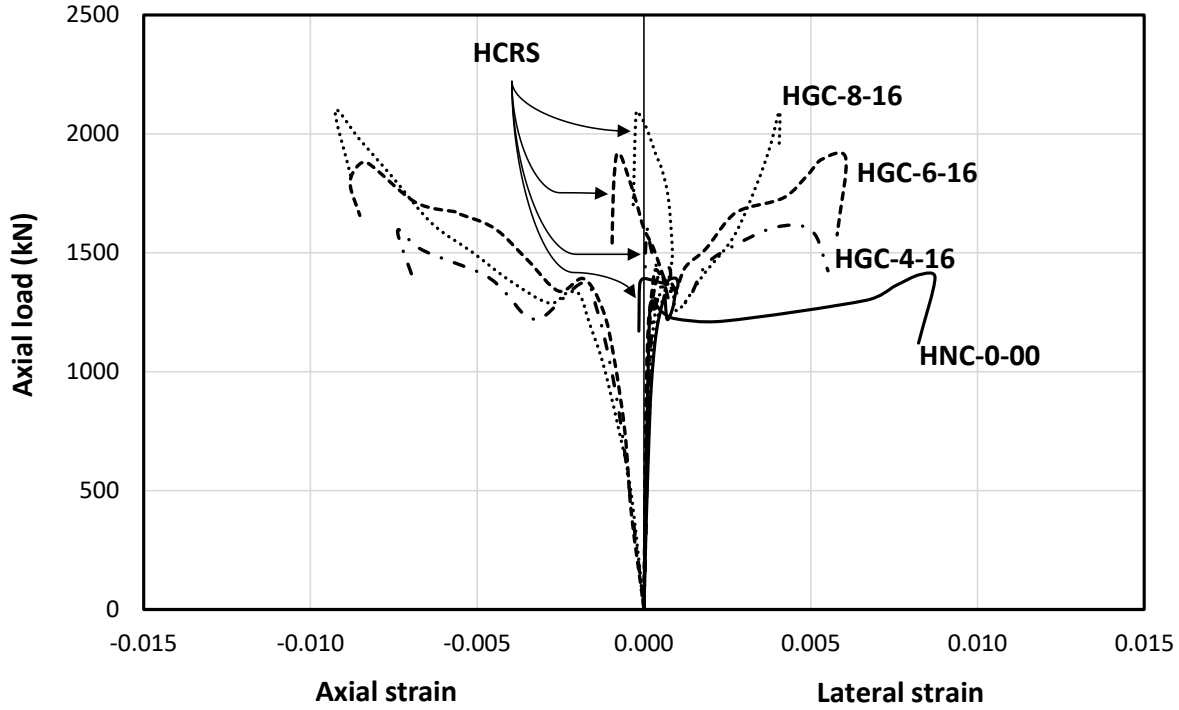

Figure 10. Axial load–strain behavior of the GFRP bars, spirals, and HCRS in Group 2

Group 3

Failure mode

Group 3 columns (HGC-6-13, HGC-6-16, and HGC-6-19) exhibited nearly the same final failure that was observed for columns reinforced longitudinally with GFRP bars. Similarly to the columns in Group 2, the progressive failure was significantly different, as shown in **Figure 11**. Column HNC-0-00 had longitudinal cracks along the column height, followed by concentrated cracks close the mid-height zone that resulted from cross-sectional bulging (see **Figure 11.a**). This behavior ended with fracturing in the lateral GFRP spirals. On the other hand, using six 13 mm GFRP bars in column HGC-6-13 resulted in a clear crack distribution along the column height, as seen in **Figure 11.b**. This behavior is due to good distribution of the smaller-diameter longitudinal GFRP bars (having low axial stiffness) around the perimeter of the concrete core. These bars were exposed to lateral expansion leading to the initiation of hairline cracks. The increased axial stiffness of the longitudinal reinforcement from providing six 16 mm diameter GFRP bars reduced the number of cracks due the larger diameter bars

having greater load-carrying capacity than the smaller diameter ones in mitigating concrete stress (see **Figure 11.c**). Providing six 19 mm diameter GFRP bars conferred higher axial stiffness to the column, limiting the crushing zone in the top portion of the column and preventing cracks from propagating downward (see **Figure 11.d**).

a. HNC-0-00 b. HGC-6-13 c. HGC-6-16 d. HGC-6-19

Figure 11. Failure progression of the columns in Group 3

Axial load–axial displacement behavior

Figure 12 shows the axial load–displacement behavior of the Group 3 columns; **Table 3** provides the column test results. A 3.6% increase in axial stiffness resulted from providing six 13 mm diameter GFRP bars in column HGC-6-13 compared to HNC-0-00. An additional 5.9% increase in axial stiffness resulted from increasing the bar diameter from 13 mm to 19 mm. These increases in axial stiffness were almost equivalent to the increase in the stiffness of the area of longitudinal GFRP bars (3.4% and 4.6%, respectively, as calculated in the preceding sections). Providing six 13 mm bars in column HGC-6-13 increased P_1 by 4.8%, which is equivalent to the load-carrying contribution of these GFRP bars at P_1. Increasing the diameter from 13 mm to 19 mm considerably increased P_1 by 13.6%. This increase indicates a combination between the load-carrying contribution of the additional reinforcement area by 8.5%, and the axial stability of the column obtained by using bigger bar diameter. This finding

is supported by the observation made by Alajarmeh et al. [17] for HCCs reinforced with different diameters of GFRP bars but no inner HCRS.

Due to the concrete cover crushing, the axial-load resistance decreased by 6.6%, 4.5%, 3.3%, and 3.6% for HNC-0-00, HGC-6-13, HGC-6-16, and HGC-6-19, respectively. Providing longitudinal GFRP bars and increasing the diameter of the GFRP bars maintained higher axial-load resistance. This finding rests on the increased area of GFRP reinforcement, which added more axial stability to the HCC due to its linear elastic behavior. Moreover, the axial stiffness at the post-peak stage was significantly maintained after the concrete cover spalled due to the effective lateral confinement provided by the GFRP spirals and longitudinal GFRP bars. Therefore, column HGC-6-13 exhibited an increase in axial stiffness of about 195% in the post-peak behavior compared to column HNC-0-00. Nevertheless, the bar diameter had no significant effect on stiffness in the post-peak stage, similar to what was observed in the linear elastic stage. This finding can be attributed to the high effective reinforcement ratio in the post-peak stage for all GFRP/HCRS-reinforced HCCs in this group (10% to 14%). The effective reinforcement ratio (ρ_e) is calculated by dividing the total area of the longitudinal GFRP bars and the HCRS on the concrete core area denoted by the distance between the spirals centers. Another reason is due to the high effectiveness of the location of the longitudinal GFRP bars, which contributed to mitigating the lateral concrete expansion and exhibited more axial stiffness. For the same reason, the increase in axial stiffness of the longitudinal GFRP bars produced by increasing the bar diameter resulted in column HGC-6-19 having only 11.5% and 11.4% increases in f'_{cc} compared to columns HGC-6-13 and HGC-6-16, respectively, even with the increase of 126% and 69% in the area of longitudinal GFRP bars, respectively. This finding is supported by the 51.4% increase in f'_{cc} for column HGC-6-19 compared to column HNC-0-00, which had no longitudinal GFRP bars. On the other hand, using the 19 mm diameter bars instead of the 13 mm diameter negatively impacted the displacement capacity. As a result,

column HGC-6-19 had 14.3% lower DF than column HGC-6-13 given that the higher reinforcement ratio yielded more energy restoration (more resistance to the axial deformation) with lower energy dissipation [34] evidenced by the lower cross-sectional lateral expansion. This can be explained by the significant reduction in the lateral expansion of column HGC-6-19, which was almost half of that of column HGC-6-13 (see ε_{s,P_2} in **Table 3**). Consequently, the comparison of GFRP/HCRS-reinforced HCCs with different bar diameters showed better load–displacement behavior, confined strength, and displacement capacity, suggesting that using a smaller bar diameter yields a more economic, efficient design to longitudinally reinforce HCCs. This is inconsistent with what Alajarmeh et al. [17] observed with GFRP-reinforced HCCs due to the presence of the HCRS, which helped inhibit lateral concrete expansion, resulting in higher energy restoration. Moreover, the HCRS prevented the inner concrete core from experiencing significant inward contraction in the post-peak behavior, allowing for greater dissipation of axial energy and greater axial deformation.

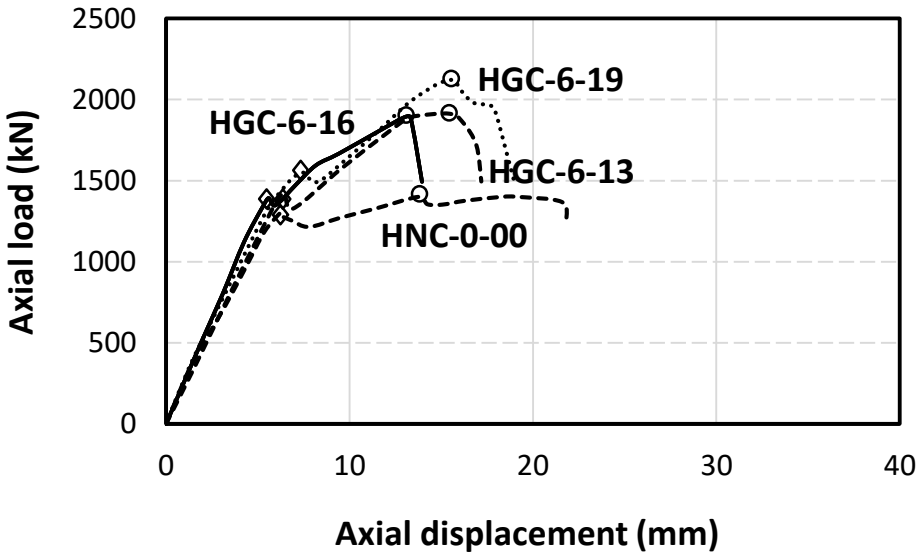

Figure 12. Load–displacement behavior of Group 3 columns

Axial load–strain behavior

Figure 13 and **Table 3** show the axial load–strain behavior of the GFRP bars, spirals, and the HCRS, as well as the strain records at the critical points on axial load–strain behavior. Similar to the other groups, the GFRP bars in **Figure 13** showed linear ascending behavior until P_1. The axial strain at P_1 (ε_{b,P_1}) ranged between 0.0020 and 0.0023. **Table 3** shows that increasing the GFRP reinforcement area (A_b) from 759 mm^2 to 1,719 mm^2 increased the gap between the concrete strain and the longitudinal GFRP bar strain at P_1. Having the longitudinal GFRP bars at the same location correlated this behavior to the reduced concrete area resulting from the increased area of longitudinal GFRP bars. This reduction increased the stress in the concrete, which led to more hairline cracks developing. Alajarmeh et al. [17] and Itakura and Yagenji [36] made similar observations. In their work, increasing the diameter of longitudinal bars produced early spreading of the hairline cracks in the concrete cover. In contrast, the lateral GFRP spirals had a hoop strain between 0.0004 and 0.0009 at P_1, which represents less than 4% of the ultimate tensile strain of the GFRP bars. The HCRS showed strain readings similar to that of the GFRP spirals, indicating the stable behavior of the concrete before reaching peak strength.

The post-peak behavior started with a significant increase in the strain readings in the GFRP bars and spirals. This increase symbolizes the role of GFRP reinforcement in maintaining axial-load resistance and in confining the remaining concrete core when the concrete shows unstable behavior, first evidenced by concrete cover crushing. Due to the unstable behavior of concrete in the post-peak stage, the HCRS was exposed to compression pressure, as seen in **Figure 13**. The increase in bar diameter decreased the ultimate compression strain in the HCRS and the inner surface of the hollow concrete section. This finding emphasizes that the increased bar diameter can reduce the confined stress in the concrete core due to higher axial stability and stiffness. The ultimate recorded compressive strain at the GFRP bars (ε_{b,P_2}) decreased with

increasing longitudinal GFRP bar diameter (see **Table 5**). This finding can be due to the column with a larger bar diameter having less deformation capacity (Δ_u) than that with a smaller bar diameter. **Figure 13** shows that increasing the reinforcement ratio reduced the ε_{s,P_2} values. Column HGC-6-19 had hoop strain 55.3% lower than column HNN-0-00. This behavior was described empirically to further demonstrate the effect of the longitudinal reinforcement on the lateral confinement produced by the lateral GFRP spirals.

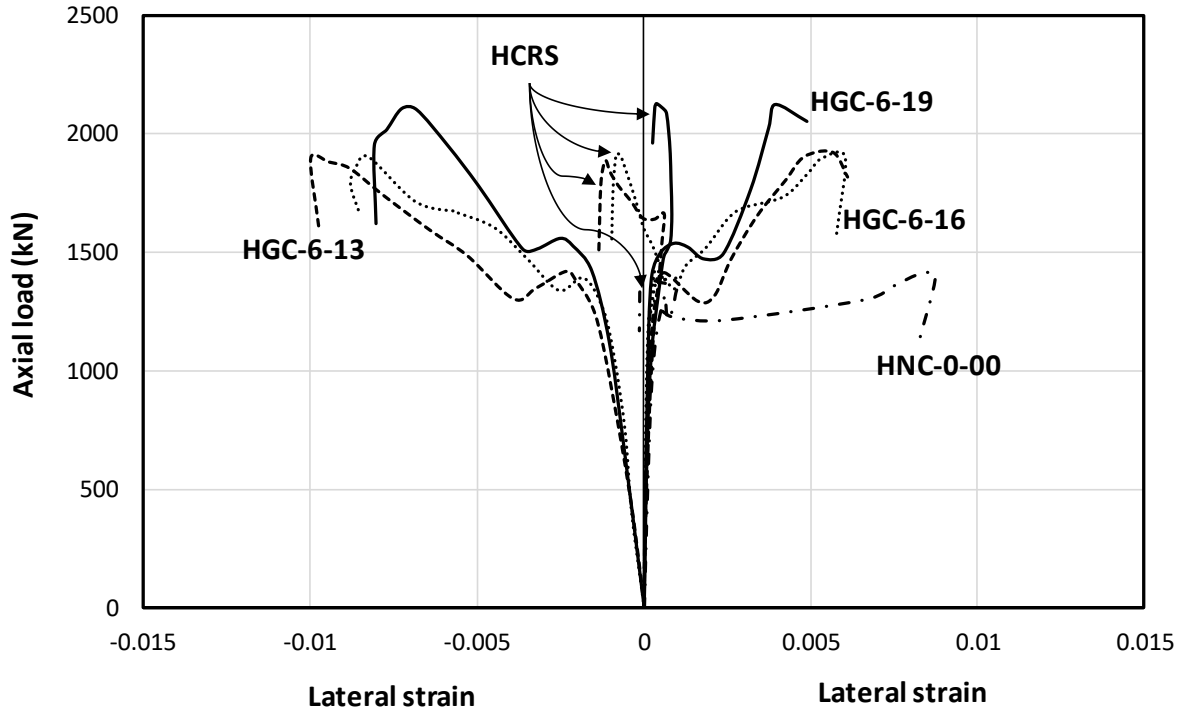

Figure 13. Axial load–strain behavior of the GFRP bars, spirals, and HCRS in Group 3

EMPIRICAL EVALUATION OF THE AXIAL BEHAVIOUR OF THE HCC'S

Theoretical design load capacity (P_n)

The design load capacity of steel-reinforced concrete columns can be estimated by considering the load-carrying contribution of the concrete and longitudinal steel bars [33]. In Eq. (2), A_c is the concrete area excluding the longitudinal reinforcement, ε_y is the yield strain of the steel bars, E_s is the modulus of elasticity of the steel bars (200 GPa), and A_s is the area of the longitudinal steel bars.

$$P_n = 0.85 \times f_c' \times A_c + \varepsilon_y \times E_s \times A_s \quad \text{Eq. (2)}$$

The concept of Eq. (2) has been adopted mostly by researchers investigating GFRP-reinforced concrete columns, where the contribution of the concrete remains similar. That notwithstanding, the load-carrying capacity of longitudinal GFRP bars accounts for their linear elastic ascending behavior [37]. A research study [38], however, calculated the load-carrying contribution of the longitudinal GFRP bars at an axial strain of 0.002, considering the strain of the concrete at peak strength, while others [1] suggested using 0.0025, which is the average of axial-strain values for a number of concrete columns at P_1. Some researchers [17, 39] have also suggested using a strain of 0.003, expressing the ultimate compressive strain of the concrete as recommended in the ACI code [33]. From these different assumptions, it can be concluded that the load-carrying capacity of the longitudinal GFRP bars can be correlated with that of concrete.

The experimental results show that the strain at concrete peak strength was almost the same for the longitudinal GFRP bars at P_1. Based on the values of the concrete compressive strength (f_c'), several concrete models were developed to describe concrete stress–strain behavior. Nevertheless, Legeron and Paultre [40] proposed a unified model for concrete considering the unconfined and confined concrete cases, which also accounted for the differences between small concrete cylinders and large-scale specimens. In this model, the strain corresponds to the concrete peak strength, as presented in Eq. (3), and has been used in the design load capacity (P_n) equation as a variable depending on f_c' value (Eq. (4)). Equation (4) is proposed for the design load capacity of the tested columns. The contribution of the GFRP bars and HCRS was calculated by considering the linear behavior of the composite reinforcement and multiplying by the concrete strain at peak strength. This implementation (Eq. (4)) is quite consistent with the experimental data, as shown in **Table 4**.

$\varepsilon_c = 0.0005 \times (f_c')^{0.4}$ [40] Eq. (3)

$P_n = 0.85 \times f_c' \times A_c + \varepsilon_c \times (E_b \times A_b + E_H \times A_H)$ Eq. (4)

Table 4. Comparison between the theoretical and the experimental design load capacity

Specimen Label	Design Load Capacity (P_n) (kN)	(P_n/P_1)
HNN-0-00	1182.7	1.11
HNC-0-00	1291.3	0.99
HGN-6-16	1291.9	0.98
HGC-6-16	1400.5	1.00
HGC-4-16	1364.1	0.98
HGC-8-16	1436.9	1.08
HGC-6-13	1360.9	0.99
HGC-6-19	1448.9	0.93

Strength Confinement Model

Lateral confinement was activated by the GFRP spirals once the concrete cover started to spall off, indicating lateral expansion in the concrete. Therefore, the columns confined with GFRP spirals tended to exhibit a second peak load and/or delayed failure by preventing the concrete core from failing. It is commonly accepted that the lateral reinforcement contributes to the whole strength confinement process. Longitudinal reinforcement, however, has also been found to play a considerable role in that process [17]. Our study also revealed the major contribution of the longitudinal reinforcement in enhancing column overall behavior. The confined strength (f_{cc}') was also found to be equal to the contribution of longitudinal reinforcement plus the strength of the confined concrete core. The existing analytical models [5, 41] could not predict the f_{cc}' values for the tested columns in this study as they consider only the effect of the lateral reinforcement, whereas it is constant in this study. The main reason could be that most of these models were established for steel-reinforced concrete columns. In

such columns, the lateral steel reinforcement provides no additional resistance once the yield strain has been reached, which is contrary to the linear elastic behavior of lateral GFRP reinforcement. Furthermore, test results in this study show that the HCRS contributed significantly as longitudinal reinforcement in the GFRP-reinforced HCCs. This finding can be explained mechanically by the low hoop strain in the HCRS compared to the high hoop strain in the GFRP spirals. This indicates that the section underwent biaxial stress, as evidenced by the nonuniform radial stress through the thickness of the concrete core. The maximum value occurred at the outer boundary and the minimum at the inner boundary, as Young et al. [42] also observed.

Alajarmeh et al. [17] recently developed a confinement model for HCCs reinforced only with GFRP bars, considering the effect of the inertia of the longitudinal GFRP bars on the confined concrete strength. This model was modified to include the contribution of HCRS as longitudinal reinforcement with different levels of axial stiffness and takes into account the effect of the longitudinal reinforcement area on hoop stress. The load-carrying contribution of the longitudinal reinforcement and concrete core were also considered in predicting the f'_{cc} values. The load contribution of the former can be easily found by multiplying the average axial strain in the longitudinal reinforcement at P_2 ($\varepsilon_{avg} = 0.00889$ with a standard deviation of 0.00103) by its modulus of elasticity and cross-sectional area (GFRP bars and HCRS), ($\varepsilon_{avg}(A_b E_b + A_R E_R)$). The concrete's load contribution is based on the effective lateral confining stress (f_{le}) induced by the GFRP spirals. Lateral confining stress (f_l) can be found in Eq. (5), while the mechanical concept is presented in **Figure 14.a**. It should be mentioned that Eq. (5) can be adopted only for fully confined cases, either by wrapping or jacketing the whole outer surface. Using discrete GFRP spirals, however, provides partial lateral confinement (see **Figure 14.b**), so a confinement effectiveness factor (k_e) (Eq. (6)) was applied to represent the true confinement process. As was also observed, the increase in the longitudinal reinforcement

area reduced the lateral expansion of the column cross section, as evidenced by the lower hoop strain in the GFRP spirals. Therefore, the longitudinal reinforcement area was plotted against the strain of the lateral spirals (denoted by ○). A good relationship between the two variables resulted in suggesting the hoop reduction factor (k_h) (Eq. (8)). Other GFRP-reinforced columns from a past study [17] were added to **Figure 15** (denoted by Δ) which showed a similar trend leading to a more reliable relationship. In **Figure 15**, the longitudinal reinforcement area in the x-axis is designated as the transformed longitudinal reinforcement area (A_t). This terminology was suggested due to the different levels of axial stiffness in the GFRP bars and HCRS, where A_t can be calculated with Eq. (7).

Past studies [17,43] found that the increase in the reinforcement ratio of the GFRP-reinforced HCCs reduced the stress contribution of the confined concrete core due to the increase in the axial stiffness of the GFRP bars. We observed something similar in this study, in which the ratio between the confined concrete strength-to-concrete compressive strength ($\frac{f_{ce}}{f'_c}$) was reduced as A_t increased (see **Figure 15**, represented by ×). This reduction in $\frac{f_{ce}}{f'_c}$ depends on the reduction factor (k_b), which takes into account the effect of the axial stiffness of the longitudinal GFRP bars on the confined concrete core, as represented in Eq. (9). Accordingly, the effective lateral confinement stress (f_{le}) is the product of multiplying the full lateral confinement stress (f_l) by the proposed reduction factors (Eqns. (6-9)) (see Eq. (10)). Afterwards, the relationship between f_{le} and f_{ce} was plotted, resulting in a good analytical interpretation, as shown in **Figure 16**. This yielded in good agreement between the experimental confined strength (f'_{cc}) values and the theoretical ones (f'_{cct}), as reported in **Table 5**. The slight discrepancy between the theoretical and experimental results is due to considering the average strain value of the longitudinal GFRP bars at f'_{cc}.

$$f_l = \frac{2A_h f_{bent}}{S(D_s - D_i)} \quad (5)$$

$$k_e = \frac{A_{ce}}{A_{cc}} = \frac{\frac{\pi}{4}\left(\left(D_s - \frac{s'}{4}\right)^2 - D_i^2\right)}{\frac{\pi}{4}(D_s^2 - D_i^2)(1-\rho_e)} \quad (6)$$

$$A_t = A_b + \frac{E_b}{E_R} A_R \quad (7)$$

$$k_h = \frac{\varepsilon_{ts}}{\varepsilon_u} = \frac{9848 - 2.12A_t}{\varepsilon_u} \quad (8)$$

$$k_b = 1.98 - \frac{4A_t}{10000} \quad (9)$$

$$f_{le} = k_e \times k_s \times k_b \times f_l \quad (10)$$

$$f_{ce} = 2.38 f_{le} + 22.81 \quad (11)$$

$$f'_{cct} = \frac{f_{ce}A_{cc} + \varepsilon_{avg}(A_b E_b + A_R E_R)}{A_g} \quad (12)$$

In Eqns. (5-12), A_h is the cross-sectional area of the GFRP spiral; D_s is the diameter of spirals on centers; D_i is the diameter of the inner hollow section; S is the spacing between the lateral spirals on centers; s' is the clear spacing between the lateral spirals; A_{ce} is the area of the concrete core, excluding the crushed concrete part due to unconfined concrete between the spirals; A_{cc} is the concrete core area, excluding the effective reinforcement ratio of the GFRP bars and HCRS (ρ_e); A_g is the gross sectional area; ε_{ts} is the theoretical strain in the lateral GFRP spirals; A_t is the transformed area of the longitudinal reinforcement; A_b is the area of the longitudinal GFRP bars; and A_R is the area of the HCRS.

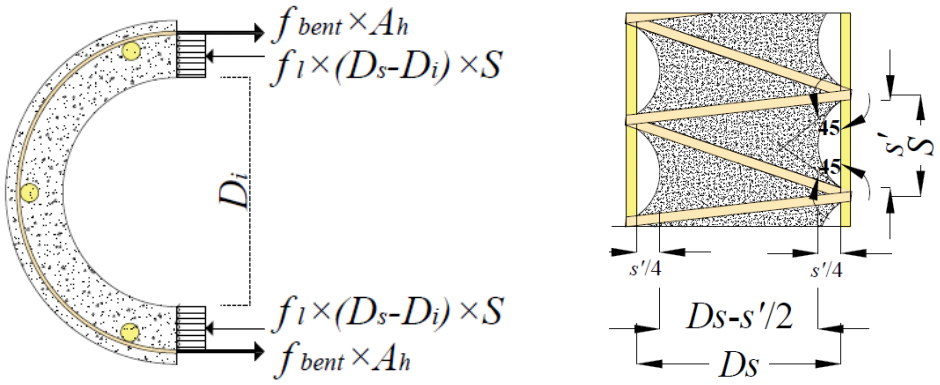

(a) Lateral-confinement mechanism **(b)** Partial lateral confinement

Figure 14. Lateral-confinement mechanism and partial lateral confinement

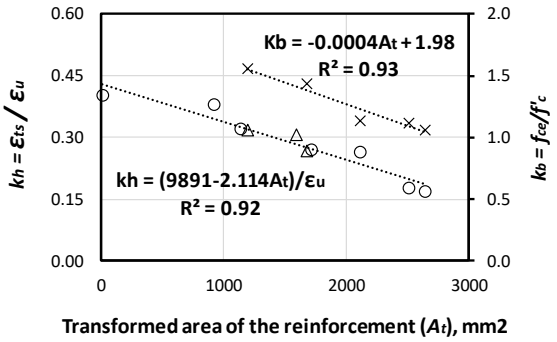

Figure 15. Effect of the longitudinal reinforcement on strength confinement

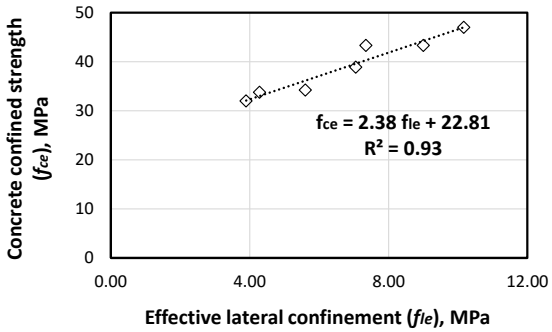

Figure 16. The relationship between f and f_{ce}

Table 5. Comparison between the theoretical and experimental confined strength

Column	k_e	k_h	k_b	f_{le} (MPa)	f_{ce} (MPa)	f'_{cct} (MPa)	f'_{cct} / f'_{cc}
HNN-0-00	0.884	0.427	1.000	9.3	43.3	44.2	1.02
HNC-0-00	0.884	0.335	1.000	6.8	38.9	56.6	1.01
HGN-6-16	0.928	0.306	1.504	9.8	47.0	70.1	0.97
HGC-6-16	0.928	0.223	1.134	5.4	34.2	77.0	1.01
HGC-4-16	0.913	0.256	1.293	6.9	30.0	72.5	1.14
HGC-8-16	0.944	0.195	0.976	4.1	33.8	82.2	0.98
HGC-6-13	0.912	0.259	1.307	7.1	43.3	72.2	0.95
HGC-6-19	0.949	0.187	0.923	3.8	32.0	84.0	0.99

CONCLUSIONS

This study presented the results of an investigation into the efficiency of reinforcing circular hollow concrete columns with different reinforcement ratios of longitudinal GFRP bars and with hollow composite-reinforced sections (HCRSs) under monotonic axial loading. Analytical interpretations were also suggested to describe the design axial load capacity and predict the strength confinement provided by the GFRP spirals. Based on the results of this study, the following conclusions were reached:

1. Providing HCRSs in the HCCs made the columns experience progressive failure compared to the columns without HCRSs. Moreover, the HCRS increased the first and second peak loads as well as the displacement capacity of the HCC by 23%, 29%, and

12%, respectively, compared to the columns without HCRSs. This was due to the section's higher axial stiffness.

2. The longitudinal GFPR bars in the HCCs significantly changed the failure mode from concrete-core crushing (plain-concrete column) to reinforcement failure. This mechanism enhanced the load–displacement behavior in terms of 23%, 66%, and 126% higher design load capacity, confined strength, and ductility, respectively.
3. Reinforcing the HCCs with longitudinal GFRP bars was more efficient and effective than using an HCRS due to the bars having higher elastic modulus (60 GPa) and strength capacity. Moreover, the GFRP bars not only resisted the axial load but provided significant lateral confinement by covering more unconfined concrete core between the GFRP spirals due to their location and arrangement. As a result, the HCC with bars exhibited 29% and 101% higher confined strength and displacement capacity than the one with an HCRS.
4. Increasing the number of longitudinal GFRP bars allowed more crack propagation and significant concrete cover crushing. Increasing the number of longitudinal GFRP bars from 4 to 8 had no insignificant effect on the design load capacity because it widened the distance between the concrete cover and the concrete core. This increase significantly increased the confined strength and ductility by 31% and 37%, respectively.
5. Adopting a larger bar diameter (19 mm instead of 13 mm) with the same arrangement limited the crack progression on the outer concrete cover due to localized column failure. Increasing the bar diameter from 13 mm to 19 mm increased the confined strength by 12% but reduced the displacement capacity by 14% due to the increased axial stiffness and reduced lateral expansion at the GFRP spirals.

6. The design load capacity of the GFRP-reinforced HCCs depended significantly on concrete behavior at crushing. Therefore, the load contribution of the longitudinal GFRP bars and the HCRS can be accurately predicted by considering the axial strain of the concrete at peak.
7. A new confinement model that takes into account the confinement effectiveness of the GFRP spirals and the axial stiffness of the longitudinal composite reinforcement can reliably predict the maximum confined strength of GFRP/HCRS-reinforced HCCs.

Future research should be conducted considering high-strength concrete with the same reinforcing system. This could provide a clearer picture of the axial contribution of composite reinforcement and its role in axial stability. Furthermore, larger cross sections can be adopted to correlate with the size effect for such columns.

ACKNOWLEDGMENTS

We are grateful to Pultrall Canada and Inconmat V-ROD Australia for providing the GFRP bars and spirals, and to Composite Reinforcement Solutions for providing the HCRSs. The assistance of the students and technical staff at the Centre of Future Materials (CFM) is acknowledged. The authors would also like to acknowledge and thank the University of Southern Queensland for providing the financial support for this project.

REFERENCES

1. AlAjarmeh, O.S., A Manalo, B Benmokrane, K Karunasena, P Mendis, and K Nguyen, *Compressive behavior of axially loaded circular hollow concrete columns reinforced with GFRP bars and spirals.* Construction and Building Materials, 2019a. **194**: p. 12-23.
2. AlAjarmeh, O.S., A Manalo, B Benmokrane, K Karunasena, W Ferdous, and P Mendis, *Hollow concrete columns: Review of structural behavior and new designs using GFRP reinforcement.* Engineering Structures, 2020. 203: p. 109829.
3. Zahn, F., R. Park, and M. Priestley, *Flexural strength and ductility of circular hollow reinforced concrete columns without confinement on inside face.* Structural Journal, 1990. **87**(2): p. 156-166.
4. Whittaker, D., R. Park, and A. Carr. *Experimental tests on hollow circular concrete columns for use in offshore concrete platforms*. in *Pacific Conference on Earthquake Engineering*. 1987.

5. Mander, J., M. Priestley, and R. Park, *Behaviour of ductile hollow reinforced concrete columns.* Bulletin of the New Zealand National Society for Earthquake Engineering, 1983. **16**(4): p. 273-290.
6. Lee, J.-H., J.-H Choi, D.-K Hwang, and I.-J Kwahk, *Seismic performance of circular hollow RC bridge columns.* KSCE Journal of Civil Engineering, 2015. **19**(5): p. 1456-1467.
7. Hoshikuma, J.-i. and M. Priestley, *Flexural behavior of circular hollow columns with a single layer of reinforcement under seismic loading.* SSRP, 2000: p. 13.
8. Ekmekyapar, T. and H.G. Hasan, *The influence of the inner steel tube on the compression behaviour of the concrete filled double skin steel tube (CFDST) columns.* Marine Structures, 2019. **66**: p. 197-212.
9. Hasan, H.G., T. Ekmekyapar, and B.A. Shehab, *Mechanical performances of stiffened and reinforced concrete-filled steel tubes under axial compression.* Marine Structures, 2019. **65**: p. 417-432.
10. Hasan, H.G., and T, Ekmekyapar, *Mechanical Performance of Stiffened Concrete Filled Double Skin Steel Tubular Stub Columns under Axial Compression*. KSCE Journal of Civil Engineering, 2019. **23**(5):2281-2292.
11. Verma, S.K., S.S. Bhadauria, and S. Akhtar, *Monitoring corrosion of steel bars in reinforced concrete structures.* The scientific world journal, 2014. **2014**: p. 9.
12. Cassidy, M., J. Waldie, and S. Palanisamy, *A Method to Estimate the Cost of Corrosion for Australian Defence Force Aircraft.* 2015.
13. Gooranorimi, O. and A. Nanni, *GFRP reinforcement in concrete after 15 years of service.* Journal of composites for construction, 2017. **21**(5): p. 04017024.
14. Mufti, A.A. and K.W. Neale, *State-of-the-art of FRP and SHM applications in bridge structures in Canada.* Composites & Polycon, The American Composites Manufacturers Association, Tampa, FL USA, 2007.
15. Benmokrane, B., C Nazair, M Loranger, and A Manalo, *Field Durability Study of Vinyl-Ester–Based GFRP Rebars in Concrete Bridge Barriers.* Journal of Bridge Engineering, 2018. **23**(12): p. 04018094.
16. Manalo A, G. Maranan, B. Benmokrane, P. Cousin, O. Alajarmeh, W. Ferdous, R. Liang, G. Hota, *Comparative durability of GFRP composite reinforcing bars in concrete and in simulated concrete environments.* Cement and Concrete Composites, 2020. **109**:103564.
17. AlAjarmeh, O.S., A Manalo, B Benmokrane, K Karunasena, W Ferdous, and P Mendis, *Axial performance of hollow concrete columns reinforced with GFRP composite bars with different reinforcement ratios.* Composite Structures, 2019b. **213**(1): p. 12.
18. AS3600, *Reinforced Concrete Design: in accordance with AS 3600-2009*. SAA HB; 71-2011, ed. L. Standards Australia, C. Cement, and A. Aggregates. 2011, Sydney, N.S.W: Cement & Concrete Aggregates Australia: Standards Australia.
19. Kupfer, H.B. and K.H. Gerstle, *Behavior of concrete under biaxial stresses.* Journal of the Engineering Mechanics Division, 1973. **99**(4): p. 853-866.
20. AS 1012.9, *Methods of Testing Concrete - Determination of the Compressive Strength of Concrete Specimens.* Australian Standards, Australian Government, 2014.
21. ASTM D695-10, *Standard Test Method for Compressive Properties of Rigid Plastics.* ASTM International, West Conshohocken, PA, 2010.
22. CSA, *Design and construction of building structures with fibre-reinforced polymers*. 2012: Canadian Standards Association, CAN/CSA-S806-12, Rexdale, ON, Canada.
23. ASTM D7205/D7205M-06, *Standard Test Method for Tensile Properties of Fiber Reinforced Polymer Matrix Composite Bars.* ASTM International, West Conshohocken, PA, 2016.
24. ACI, *Guide for the Design and Construction of Concrete Reinforcedwith FRP Bars (440.1R-15).* American Concrete Institute, Farmington Hills, MI, 2015.
25. AlAjarmeh, O.S., A Manalo, B Benmokrane, K Karunasena, and P Mendis, *Effect of Spiral Spacing and Concrete Strength on Behavior of GFRP-Reinforced Hollow Concrete Columns.* Journal of Composites for Construction, 2019. 24(1): p. 04019054.
26. AlAjarmeh O.S., A.C.M., B. Benmokrane, P.V. Vijay, W. Ferdous, P. Mendis, *Novel testing and characterization of GFRP bars in compression.* Construction and Building Materials, 2019. **Volume 225**: p. Pages 1112-1126.

27. CSA, *Canadian highway bridge design code. Rexdale, ON, Canada: CAN/CSA S6-14*. 2014: p. 733.
28. Sankholkar, P.P., *Confinement model for concrete columns internally reinforced with glass fiber reinforced polymer spirals*. 2016, The University of Utah.
29. Al-saadi, A.U., T. Aravinthan, and W. Lokuge, *Effects of fibre orientation and layup on the mechanical properties of the pultruded glass fibre reinforced polymer tubes.* Engineering Structures, 2019. **198**: p. 109448.
30. Fam, A. and S.H. Rizkalla, *Behavior of axially loaded concrete-filled circular FRP tubes.* ACI Structural Journal, 2001. **98**(3): p. 280-289.
31. Afifi, M.Z., H.M. Mohamed, and B. Benmokrane, *Theoretical stress–strain model for circular concrete columns confined by GFRP spirals and hoops.* Engineering Structures, 2015. **102**: p. 202-213.
32. Cascardi, A., F. Micelli, and M.A. Aiello, *Unified model for hollow columns externally confined by FRP.* Engineering Structures, 2016. **111**: p. 119-130.
33. ACI, *(American Concrete Institute), Building code requirements for structural concrete.* ACI 318-14M, Farmington Hills, MI, 2014.
34. Hadi, M.N., H.A. Hasan, and M.N. Sheikh, *Experimental Investigation of Circular High-Strength Concrete Columns Reinforced with Glass Fiber-Reinforced Polymer Bars and Helices under Different Loading Conditions.* Journal of Composites for Construction, 2017: p. 04017005.
35. Mo, Y., D. Wong, and K. Maekawa, *Seismic performance of hollow bridge columns.* Structural Journal, 2003. **100**(3): p. 337-348.
36. Itakura, Y. and A. Yagenji, *Compressive test on high-strength R/C columns and their analysis based on energy concept.* Notes, 1992. **8**(C8P9D): p. C8P9D.
37. Hasan, H.A., M.N. Sheikh, and M.N. Hadi. *Maximum axial load carrying capacity of Fibre Reinforced-Polymer (FRP) bar reinforced concrete columns under axial compression*. in *Structures*. 2019. Elsevier.
38. Tobbi, H., A.S. Farghaly, and B. Benmokrane, *Behavior of concentrically loaded fiber-reinforced polymer reinforced concrete columns with varying reinforcement types and ratios.* ACI Structural Journal, 2014. **111**(2): p. 375.
39. Hadi, M.N., H. Karim, and M.N. Sheikh, *Experimental investigations on circular concrete columns reinforced with GFRP bars and helices under different loading conditions.* Journal of Composites for Construction, 2016. **20**(4).
40. Légeron, F. and P. Paultre, *Uniaxial confinement model for normal-and high-strength concrete columns.* Journal of Structural Engineering, 2003. **129**(2): p. 241-252.
41. Lignola, G.P., A Porta, G Manfredi, and E Cosenza, *Unified theory for confinement of RC solid and hollow circular columns.* Composites Part B: Engineering, 2008. **39**(7): p. 1151-1160.
42. Young, W.C., R.G. Budynas, and A.M. Sadegh, *Roark's formulas for stress and strain*. Vol. 7. 2002: McGraw-Hill New York.
43 Alajarmeh O., AC. Manalo, B. Benmokrane, W. Karunasena, W. Ferdous, P. Mendis, *A New Design-Oriented Model of Glass Fiber-Reinforced Polymer-Reinforced Hollow Concrete Columns.* ACI Structural Journal, 2020. **117**(2).